2008

Effects of nanoscale disorder on the paramagnetic to ferromagnetic transition in melt-spun gadolinium and gadolinium iron alloys

Justin Gary Bohnet
University of Northern Iowa

THE EFFECTS OF NANOSCALE DISORDER ON THE PARAMAGNETIC TO FERROMAGNETIC TRANSITION IN MELT-SPUN GADOLINIUM AND GADOLINIUM IRON ALLOYS

A Thesis

Submitted

in Partial Fulfillment

of the Requirements for the Designation

University Honors

Justin Gary Bohnet

University of Northern Iowa

May 2008

Overview:

As nanoscale science continues to flourish, scientists strive to understand how structure and order (or disorder) on the nanoscale contribute to macroscopic properties, such as magnetism. This study examines alloys of gadolinium and iron that have been nanostructured through the process of melt-spinning. The result was a two-part system consisting of small (~70 nm) gadolinium grains surrounded by an amorphous gadolinium and iron matrix. Measurements of the samples' DC magnetization and AC susceptibility were performed. By looking at the paramagnetic to ferromagnetic transition in the materials, the critical exponents were obtained and used to classify and understand how the addition of iron and the melt-spinning process affected the magnetic properties. By using relatively simple magnetic atoms, we intend for this study to be a fundamental look at disorder on the nanoscale and a model system for future investigations.

Introduction and motivation:

Significant advances in technology, particularly in data processing and communications, have been made possible by fundamental research in magnetism. This research has led to discoveries of magnetic behaviors such as giant magnetoresistance (GMR), which recently won a Nobel Prize in physics [1]. As scientists continue to investigate magnetic systems, much attention has been given to nanoscale structures, which are technologically promising and are also extremely interesting from the point of view of fundamental science. For example, the phenomenon of colossal magnetoresistance is thought to derive much of its rich complexity from nanoscale structures and their interactions [2] [3] [4]. Nanoscale systems are generally defined to be systems in which at least one dimension has a size of less than 100 nanometers (10^{-9} meters). As the size of the system is reduced to the nanoscale, the surface area to volume ratio increases dramatically, affecting the environment of the electrons. As the electron is the generator of the electric and magnetic properties, this size reduction can have significant effects on the properties of materials.

Interesting effects of imperfections and disorder –a characteristic of many nanoscale systems– on bulk magnetic properties, especially magnetic phase transitions, have also been observed recently [5]. Disordered magnetic materials display a range of interesting and useful magnetic and electronic properties, because the arrangement of atoms in a material and the interactions between them play a significant role in the emergence of these phenomena. Introducing disorder into a system affects this arrangement, and thereby affects the material's properties. Disorder in a magnetic system can be classified as chemical disorder, in which an atom or ion replaces another in a crystal lattice, or structural disorder, in which an atom or ion is moved from its place in a crystal lattice. Structural disorder can vary from the entire breakdown

of the crystal lattice seen in an amorphous material, to something more intermediate, such as crystal grain surrounded by amorphous regions.

Gadolinium (Gd) metal provides the basis for all the samples studied in this project. It crystallizes in a hexagonal close packed structure, with the lattice constants a = 0.3629 nm and c = 0.5795 nm [6]. One of the first studies ever published on Gd is by Nigh, Legvold, and Spedding, where it was shown that Gd is a prototypical ferromagnet with a Curie temperature (T_c) of 293.2 K and an effective magnetic moment per atom of 7.98 Bohr magnetons (the magnetic moment of one electron) near the transition [7]. (The Curie temperature is the temperature at which there is a transition between the paramagnetic and ferromagnetic phases.) Dan'kov et al. demonstrated that T_c is 294(1) K, independent of the method of analysis [8], and Nigh et al. provided a careful study of the phase transition, showing the paramagnetic to ferromagnetic transition took the form of a sharp, second-order phase transition [7]. Because the ferromagnetism in Gd arises from well-localized Gd magnetic moments, it provides a good control for examining disordered magnetic systems. Recently, Michels, Krill, and Birringer have performed measurements on nanocrystalline Gd prepared by inert-gas condensation methods [9]. This method resulted in a polycrystal with randomly oriented nanometer-sized grains surrounded by a network of grain boundary regions [9]. The grain sizes in these studies varied from 8 nm to 150 nm. Using Mössbauer spectroscopy, Michels et al. found that the T_c decreases as the grain size is reduced. They also found that the spontaneous magnetization was best described as being composed of a component from the crystalline grains and a component from the disordered grain boundaries. The decrease in T_c explained in terms of pressure applied on the grains by the grain boundaries, which is consistent with behavior of bulk Gd [10]. Dun-hui et al. also showed that

the FM-PM transition in a melt-spun Gd sample took place near the same T_c as bulk Gd, but the transition was significantly broadened [11].

One can introduce disorder into a magnetic system by inserting another element into the material's lattice as well as by displacing the atoms from their regular spacing [12]. Amorphous materials are structurally disordered systems, because the atoms no longer reside in a lattice structure that repeats throughout the material. By adding some Gd to iron (Fe), an amorphous alloy with chemical disorder can be produced by melt-spinning [13]. Yano et al. reported that the crystal structure of melt-spun Gd-Fe samples containing a percentage of Gd ranging from 18 to 60 percent was determined by x-ray diffraction techniques to be amorphous. A study by Petkov, Yano, and Kita also used x-ray diffraction to show that melt-spun (or rapid melt quenched, to use their terminology) Gd-Fe alloys were amorphous [14]. In addition, it was demonstrated that melt-spinning produced an amorphous structure distinct from that of sputtering (evaporative) deposition. Varying the amount of Gd present in the sample produced differences in the amorphous structure as well. These amorphous materials were still ferrimagnetic, i.e., the exchange interaction between Gd and Fe causes the moments to align antiferromagnetically, but the unequal magnitude of the moments means that some net magnetization still survives. The FM-PM transition in these samples was broadened, and the T_c showed some dependence on the Gd concentration. Petkov, Yano, and Kita concluded that the amorphous samples are dominated by short-range interactions and random anisotropy [14]. In these samples, Fe tended to cluster, keeping the alloy from being a homogenous mixture. The work indicates that at higher Gd concentration (concentration > 60%) nanoscale grains of pure gadolinium embedded in an amorphous matrix composed of both Gd and Fe; however, studies of

nanostructured GdFe that contain a mixture of nanoscale grains and amorphous boundary regions are rare [14].

By examining gadolinium-iron alloys as prototypical systems, we seek to better understand the effects that disorder has on the properties of magnetic systems and correlate disorder to effects on the extrinsic and intrinsic magnetic properties of the bulk material. In this thesis, we present experimental data on the magnetic properties of the paramagnetic to ferromagnetic phase transition of nanostructured gadolinium (Gd) and gadolinium-iron alloys (Gd_xFe_{100-x}). The nanostructures we have studied consist of nanometer-sized crystallites or grains embedded in a disordered grain boundary (GB) region. Because the behavior of the system in the region of the phase transition is governed by spatial dimensionality, spin dimensionality, the range of the spin-spin interaction, and the strengths of coherent and random anisotropy, we can study the effects of nanoscale disorder, and the competition between the GB and the nanoscale grains, on one or more of these factors.

Theory:

Understanding the origins of magnetic phenomena begins with identifying the origin of the magnetic moment. The electron is endowed with an intrinsic angular momentum, analogous to other intrinsic quantities, such as mass and charge, which gives rise to a magnetic moment [15]. This magnetic moment is present on every electron, but its presence does not guarantee that every isolated atom will have a magnetic moment. The magnetic moment of a bare electron can take one of two values, and two electrons with opposite magnetic moments can result in a total magnetic moment of zero. If the magnetic moments of the electrons do not completely cancel, a net magnet moment can be associated with the atom or ion. A net magnetic moment will be present on atoms where the inner d- or f-electron shells are incompletely filled. When the

atom or ion is incorporated into a solid, the behavior is more complex. In a solid, the localized magnetic moments on atoms or ions are actually time-averaged results of a dynamical process [15]. For our purposes, it is useful to treat these atoms as having a permanent magnetic moment.

Materials composed of atoms with a permanent magnetic moment exhibit paramagnetism, which means that the material responds to an applied magnetic field with a magnetization that is parallel to the field. The magnetic moments tend to line up along the externally applied field, and as the individual moments begin to align, they contribute to the overall magnetization of a sample. This relation between the magnetization and the external applied field also leads to susceptibility, another important property of a magnetic material. Susceptibility, χ, is defined as:

$$\chi = M / H \tag{1}$$

where M is the magnetization and H is the external applied field [16]. The susceptibility is a measure of the difficulty in changing a material's magnetization. Another important characteristic of a material is its AC susceptibility. AC susceptibility measures a sample's response to a changing magnetic field, dH. Therefore, "true" susceptibility, χ, is sometimes called DC susceptibility. AC susceptibility does not measure a material's magnetic moment, but its change in magnetic moment, dM. Pure paramagnetic magnetization assumes that the atomic moments are isolated and do not interact. However, magnetic moments do interact, most significantly via a quantum mechanical effect known as the exchange interaction [16].

The exchange interaction couples magnetic moments in a variety of ways. Hurd describes the variety of couplings in detail [15]. For our purposes, we note that the exchange interaction can align moments in the same direction (a ferromagnetic arrangement) or in opposite directions (an antiferromagnetic arrangement). Thus, a magnetic system becomes a sort of

competition between two factors: the tendency of the exchange interaction to align (correlate) magnetic moments and the tendency of thermal fluctuations to orient the moments randomly. In some materials, at a low enough temperature, the exchange interaction overcomes thermal fluctuations and leads to a large-scale alignment of moments. There are regions (domains) containing many moments in which there is magnetization without the presence of a magnetic field. This correlated case is called ferromagnetism. The transition from paramagnetism to ferromagnetism occurs at a temperature called the Curie temperature (T_c), also known as the critical temperature [16]. The paramagnetic to ferromagnetic (PM) phase transition is indicated by a sharp increase in magnetization as the temperature is lowered and the correlation length of the system increases. Another hallmark of the PM phase transition is a peak in the ac susceptibility that is suppressed and shifted toward higher temperatures by an applied magnetic field [17].

The strength and alignment tendency of the exchange interaction can depend on the nature of the interaction, as well as the distance between the interacting moments. Thus, introducing chemical disorder, where a new atom is substituted for another in the crystal lattice, can affect the exchange interaction and possibly the transition. Similarly, changing the structure of the material affects the distances between atoms, altering the exchange interaction, which can lead to a change in the properties of the phase transition.

One way to study the physics of magnetic systems is by observing their behavior in the temperature region where the material goes through a paramagnetic to ferromagnetic transition. The transition depends on the exchange interaction and anisotropy effects, so in this critical region, system characteristics emerge, and the effects of spatial disorder may be apparent. The phase transition region is characterized according to its transition temperature and its critical

exponents, which are the exponents in the power-law behavior of the spontaneous magnetization and susceptibility expressed as functions of the reduced temperature (see below). Comparing the critical exponents to exponents obtained from other samples, as well as comparing them with values calculated from phase transition theory, can lead to insight into the mechanisms governing the phase transition.

Three important critical exponents for this study are beta (β), gamma (γ), and delta (δ). Beta is the spontaneous (zero magnetic field) magnetization exponent, which is defined by the following single power law relation:

$$M_S(T) = M_0(-\varepsilon)^{\beta}, \varepsilon < 0, \tag{2}$$

where $\varepsilon = \frac{T - T_c}{T_c}$ is the reduced temperature and M_0 is a critical amplitude. Gamma is the isothermal magnetic susceptibility exponent defined as

$$\chi_0^{-1}(T) = (h_0 / M_0)\varepsilon^{\gamma}, \varepsilon > 0 \tag{3}$$

where χ_0^{-1} is the inverse zero-field susceptibility, and h_0 is a critical amplitude.

Delta is the critical isotherm exponent:

$$M = DH^{\frac{1}{\delta}}, \varepsilon = 0 \tag{4}$$

where H is the demagnetization-adjusted applied magnetic field, and D is a critical amplitude [18]. Note that (2) and (3) are strictly valid in the limit $\varepsilon \to 0$, known as the asymptotic critical region. Equation (4) is valid exactly at $T = T_c$. Clearly, the accurate determination of T_C is of paramount importance. We will refer to these equations as the single power law equations (SPL) [12]. Note that these relations are first order approximations. It is common to refer to the additional terms as correction to scaling (CTS) terms [19].

Different model systems have different values for the critical exponents. Thus, comparing measured values with values predicted for certain models indicates the character of a transition. Two important models are the Mean Field model and the Heisenberg model. Mean field theory assumes that every moment is interacting with every other; in effect, the exchange interaction is infinitely ranged, resulting in critical exponents of $\gamma = 1$, $\beta = 0.5$, and $\delta = 3$. The Heisenberg model assumes that the exchange interaction is short-ranged and that magnetic moments are only interacting locally. The critical exponents for the short-range three-dimensional (3D) Heisenberg model are $\gamma = 1.386$, $\beta = 0.365$, and $\delta = 4.536$ [17].

Different methods exist for measuring T_c and the critical exponents. S. N. Kaul has compiled many of the methods, including methods using both DC magnetization data and AC susceptibility data [19]. The two methods of interest are what Kaul names asymptotic analysis II (AA-II), and ac susceptibility data analysis. AA-II uses the Arrott-Noakes plot [20] to extract values of M_s and χ_0^{-1}. The Arrott-Noakes plot is a graph of $M^{\frac{1}{\beta}}$ versus $\left(\frac{H}{M}\right)^{\frac{1}{\gamma}}$ that depends on the relationship

$$\left(\frac{H}{M}\right)^{\frac{1}{\gamma}} = \frac{T - T_C}{T_1} + \left(\frac{M}{M_1}\right)^{\frac{1}{\beta}} \tag{5}$$

which arises from a combination of (2) and (3) [20]. A standard Arrott plot uses mean field theory exponents ($\gamma = 1$, $\beta = 0.5$, $\delta = 3$), which are characteristic of systems with infinite-range interactions. Thus, the relationship simplifies to a graph of M^2 vs H/M. When correct exponent values are used in the Arrott-Noakes plot, the data has a linear relationship for sufficiently large fields, and the extrapolations to the axes yields the values of spontaneous magnetization M_S and

inverse zero-field susceptibility χ_0^{-1}. Note that for the isotherm at T = T_C, the y-intercept should be zero. With these zero field extrapolations, a process based on relations (2) and (3) that we call the intercept method, can be used to arrive at the best values for the critical exponents. M. Sahana gives one example of using the intercept method [18]. The extrapolations are used to determine an initial value of M_s, $1/\chi_0$, and T_c. The initial T_c is then used to determine ε. Taking the natural logarithm of both sides of (1.2) and (1.3) results in

$$\ln M_s = \ln M_0 + \beta \ln(-\varepsilon), \varepsilon < 0 \tag{6}$$

$$\ln\left(\chi_0^{-1}\right) = \ln(h_0 / M_0) + \gamma \ln(\varepsilon), \varepsilon > 0 \tag{7}$$

which allows one to do a linear plot and determine refined values of γ and β from the slope of the line. Exponents that produce linear isotherms on the Arrott-Noakes plot and are constant within uncertainty under this process are considered accurate.

The Kouvel-Fisher (KF) method [21] can also be used to determine critical exponents from these values as demonstrated in references [18], [19], and [22]. The derivatives of equations (2) and (3) are

$$\left(\frac{dM_s}{dT}\right) = M_o \beta (-\varepsilon)^{\beta-1} \tag{8}$$

$$\left(\frac{d\chi_0^{-1}}{dT}\right) = (h_o / M_0)\gamma(\varepsilon)^{\gamma-1} \tag{9}$$

Thus, dividing (2) and (3) by (8) and (9) give linear relationships

$$M_s\left(\frac{dM_s}{dT}\right)^{-1} = \frac{(T - T_c)}{\beta} \tag{10}$$

$$\chi_0^{-1}\left(\frac{d\chi_0^{-1}}{dT}\right)^{-1} = \frac{(T - T_c)}{\gamma} \tag{11}$$

The KF method uses the M_S and χ_0^{-1} taken from the AN plot and generates refined values of the critical exponents γ and β by determining the slope of a graph of $M_s\left(\frac{dM_s}{dT}\right)^{-1}$ vs T and $\chi_0^{-1}\left(\frac{d\chi_0^{-1}}{dT}\right)^{-1}$ vs T . These updated values are used to create a new AN plot. The process is repeated until the updated values are unchanged within uncertainty. The KF method, unlike the intercept method described above, has the advantage of being determined independent of a T_c estimated from interpolation. In fact, a value for T_c can be determined from the y-intercept and slope of the KF graph. However, the process depends on a numerical differentiation, which can be unreliable if enough data points are not present.

Because these procedures use the asymptotic values of magnetization and ac susceptibility, the extrapolation process is important. An alternate method for arriving at the values for M_s and χ_0^{-1} is what Kaul calls the parabolic extrapolation [19]. Kaul points out that the relationship in equation (5) is an approximation, with terms proportional to higher powers of M are neglected [19]. Under certain cases, those terms may need to be included for an accurate determination of the intercepts.

The ac susceptibility analysis can also be a useful method for determining the value of γ, as χ_0^{-1} can be taken directly from the data once a value for T_c is determined. Examples of ac susceptibility analysis include work by Zhao et al., [23] Peles [17], and Fischer, Kaul, and Kronmueller [22].

When a system undergoes a paramagnetic to ferromagnetic transition, the ac susceptibility can be written as

$$\chi'(h,t) = h^{1-1/\delta} H\left(\frac{h}{\varepsilon^{\gamma+\beta}}\right) = \varepsilon^{-\gamma} G\left(\frac{h}{\varepsilon^{\gamma+\beta}}\right) \tag{12}$$

where H(X) and G(X) are universal functions of their arguments [23]. Since ac susceptibility has a peak in a phase transition, the maximum will occur at the same value for $\frac{h}{\varepsilon^{\gamma+\beta}}$. Therefore,

$$\frac{h}{\varepsilon^{\gamma+\beta}} = C \tag{13}$$

where C is a constant. Then, the reduced temperature, ε, of the maxima of the ac susceptibility vs temperature is proportional to $H_i^{1/(\gamma+\beta)}$. Thus, we can write the actual temperature of the maximum as

$$T_m = (k * T_C)\left(H^{1/\gamma+\beta}\right) + T_C \tag{14}$$

This relationship provides another way for one to determine a critical temperature. Also, from equation (12), it follows that

$$\chi'(h,t) \propto \varepsilon^{-\gamma} \tag{15}$$

which is useful for determining the critical exponent γ directly from ac susceptibility data.

Finally, note that using one or more of these methods will yield a value for T_c that can be used to determine the exponent δ directly from experimental data and the use of equation (4) [18, 19, 17]. Scaling theory predicts a number of relationships between the critical exponents that should be true for correct experimental exponents [17]. One such relation, the Widom scaling relation, relates the values of β, γ, and δ as

$$\delta = 1 + \gamma/\beta \tag{16}$$

The Widom scaling relation will provide an important check to the values of the critical exponents obtained in our analysis.

Experimental Details

The samples were prepared using a melt-spinning apparatus at the University of Nebraska-Lincoln. The gadolinium (99.9%) was prepared for melt-spinning by arc-melting under an argon gas atmosphere. The melt-spinning was performed under a argon atmosphere on a copper disk rotating with a tangential speed of 40 m/s. The samples obtained were ribbons 7-10 mm long. X-ray diffraction (XRD) was performed with the samples mounted with silicone vacuum grease on a zero-background holder. The samples were prepared for transmission electron microscope (TEM) analysis by gluing the ribbon pieces on copper grids, then ion milling.

The magnetic measurements were performed on a Quantum Design Physical Property Measurement System, with an ACMS (AC Magnetization System) attachment. All AC susceptibility measurements were performed in an AC-driving field with amplitude of 3 Oe and a frequency of 1 kHz. AC susceptibility measurements were taken in the temperature range 2-350 K. AC susceptibility versus temperature measurements in the range 286 K-304 K were taken with superimposed DC bias fields ranging from 600-3000 Oe in increments of 200 Oe. Magnetization versus external field data for ms-Gd were taken along isotherms at intervals of 1 K from 286 K-294 K in fields up to 6 Tesla (Figure 1). The data were corrected for demagnetization; the demagnetization factor was determined using low field measurements of the magnetization versus external field and the density of the sample. After data at each temperature was taken, the sample temperature was raised to 325 K to fully demagnetize it. It was then cooled to the next temperature to be measured.

Magnetization versus external field data for the alloy samples were taken along isotherms at intervals of 0.25 K from temperatures ranging from 285.25 K to 298 K in fields up to 6 Tesla. Again, the data were corrected for demagnetization with the demagnetization factor determined as explained above.

Table 1: Physical information on samples

Sample	Mass (mg)	Composition (% nanocrystalline)	Grain Size (nm)	Demagnetization Factor (Oe*g/emu)
ms-Gd	**11.92**	**75%**	**73±5**	**1.695**
ms-$Gd_{97}Fe_3$	**0.98**	**68%**	**73±5**	**1.899**
ms-$Gd_{94.6}Fe_{5.4}$	**1.30**	**60%**	**73±5**	**2.100**
ms-$Gd_{80}Fe_{20}$	**0.88**	**35%**	**73±5**	**1.927**

Results:

I. Ms-Gd

A. Structural Properties

The structure of melt-spun Gd was determined with a combination of X-ray diffraction, transmission electron microscopy (TEM), and extended x-ray absorption fine structure (EXAFS). X-ray diffraction confirmed that the sample was composed of nanocrystalline grains, and Williamson-Hall analysis on the x-ray diffraction data indicated that the grain size was 73 ± 5 nm. TEM images confirmed that the sample consisted of crystalline grains surrounded by amorphous grain boundary regions. The TEM images indicated that the grain size was approximately 150 nm; however, this was attributed to the small region in which the image was taken. Finally, the EXAFS data shows that the majority of the sample (75%) is composed of the nanocrystalline grains of hcp-Gd. The remainder is amorphous Gd confined to the boundary regions [24].

B. DC Magnetization

In this section, we present data on the temperature variation of DC magnetization in an applied magnetic field data, which are used to determine T_C and the critical exponents γ, β, and δ by Arrott-Noakes analysis. The unmodified isotherms for magnetization versus applied field are in Figure 1.

Figure 1: Magnetization vs external field for temperatures 286-294 K.

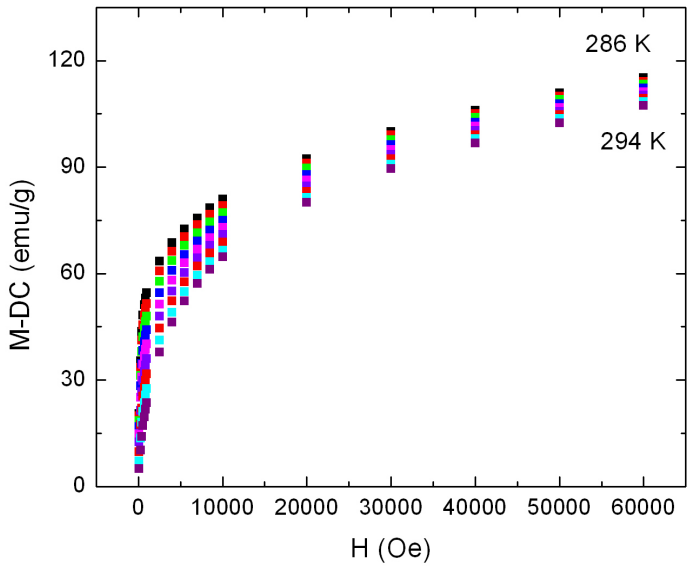

The standard Arrott plot in Figure 2 is clearly non-linear at all fields, indicating that mean field theory does not apply. In order to use the Arrott plot to determine the asymptotic values of magnetization and susceptibility, we must determine reasonable guesses for the critical exponents, then construct an AN plot.

Figure 2: Standard Arrott Plot

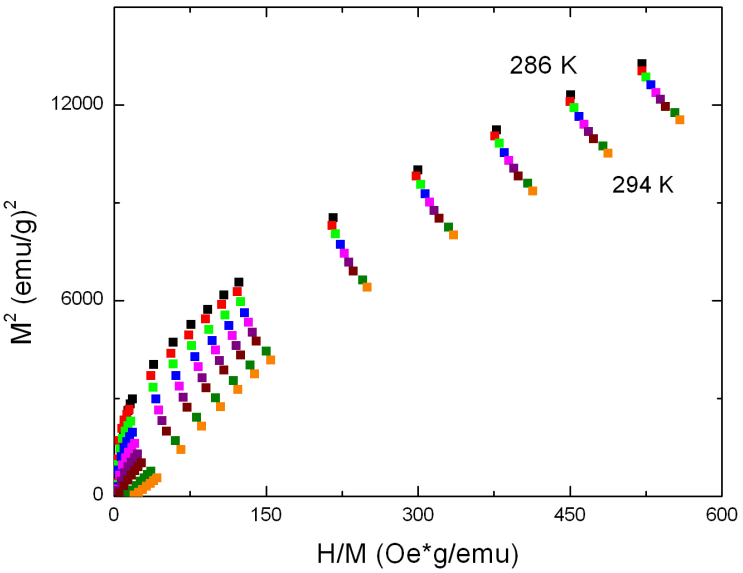

In order to determine correct values for γ and β, **(5)** was rearranged so that a nonlinear curve fitting routine could be performed on the data with gamma and beta as two of the parameters. To perform the nonlinear fit, the initial values of the critical exponents that were used were those for the classical 3D Heisenberg model with short-range interactions (β = 0.365 , γ = 1.386, δ = 4.78) [19]. This process yielded preliminary values of γ and β, which were used to generate an Arrott-Noakes plot (Figure 3).

Figure 3: Arrott-Noakes Plot

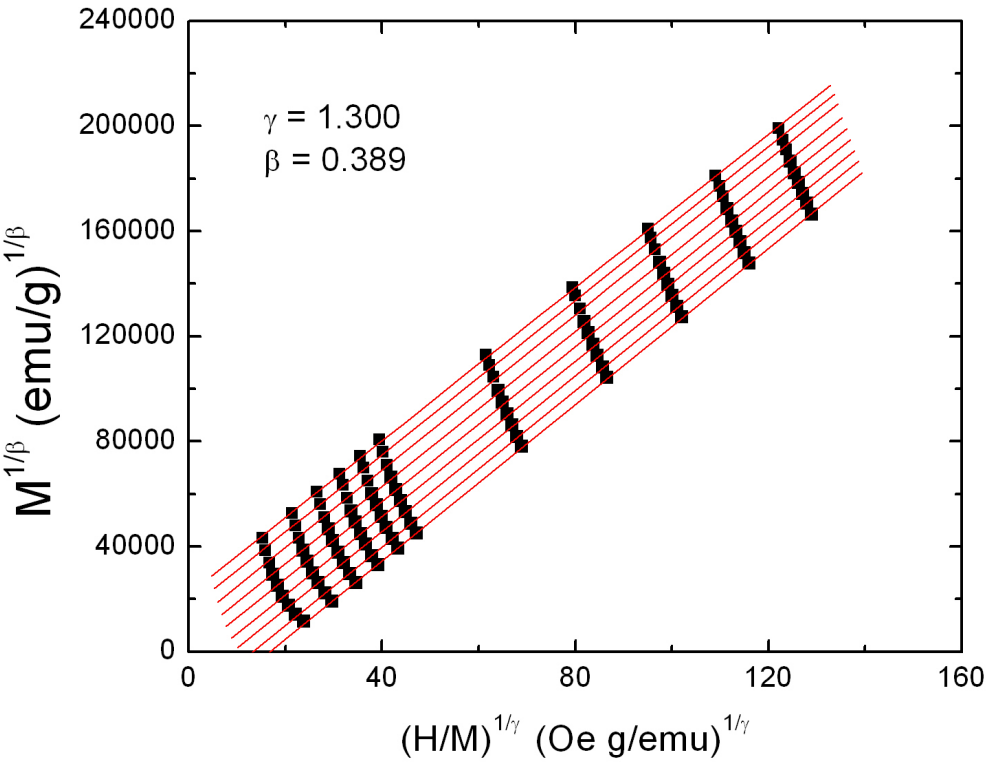

The intercepts were extrapolated and used to determine T_C, $M_S(T)$, and $\chi_0^{-1}(T)$, which were then used to generate a log-log plot (Figure 4).

Figure 4: Double logarithmic plots for the spontaneous magnetization and inverse susceptibility to determine critical exponents gamma and beta.

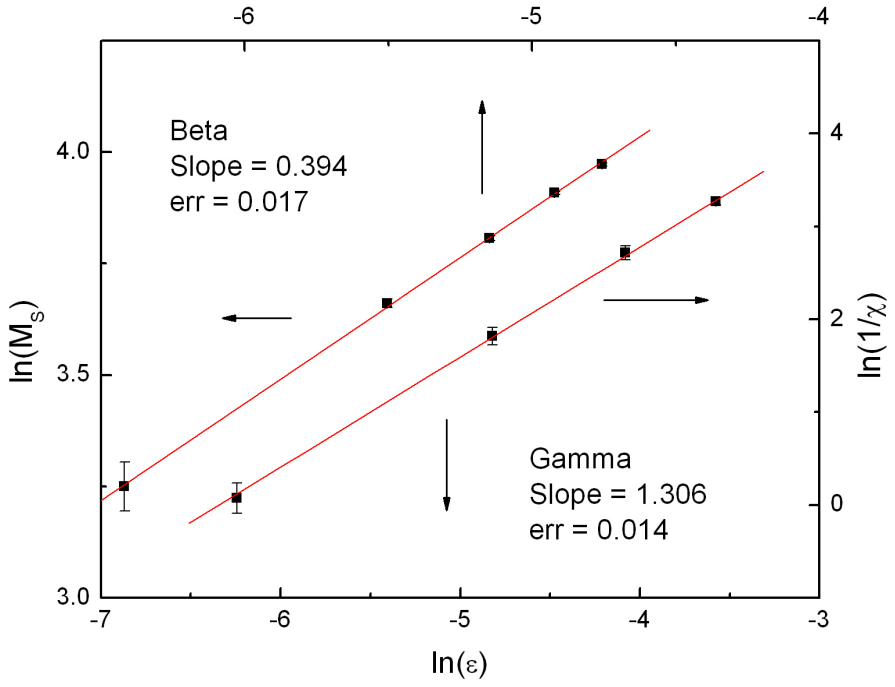

The slopes of these plots gave updated values of γ and β (see **(2)** and **(3)**). These resulting values of gamma and beta were then used to reconstruct the Arrott-Noakes and log-log plots, which updated the values of gamma and beta within uncertainty limits. The process resulted in a $\beta = 0.389 \pm 0.017$, $\gamma = 1.300 \pm 0.014$, and $T_C = 289.70 \pm 0.1$ K.

With an accurate value for T_C, the critical exponent δ can be calculated directly from the DC magnetization data on the critical isotherm with a log-log plot of magnetization versus applied field (see **(4)**). Since our data were taken at 1 degree intervals, the value of delta was interpolated from the inverse of the slope of the 290 K and 289 K isotherms (Figure 5).

Figure 5: Determining Delta on the critical isotherm

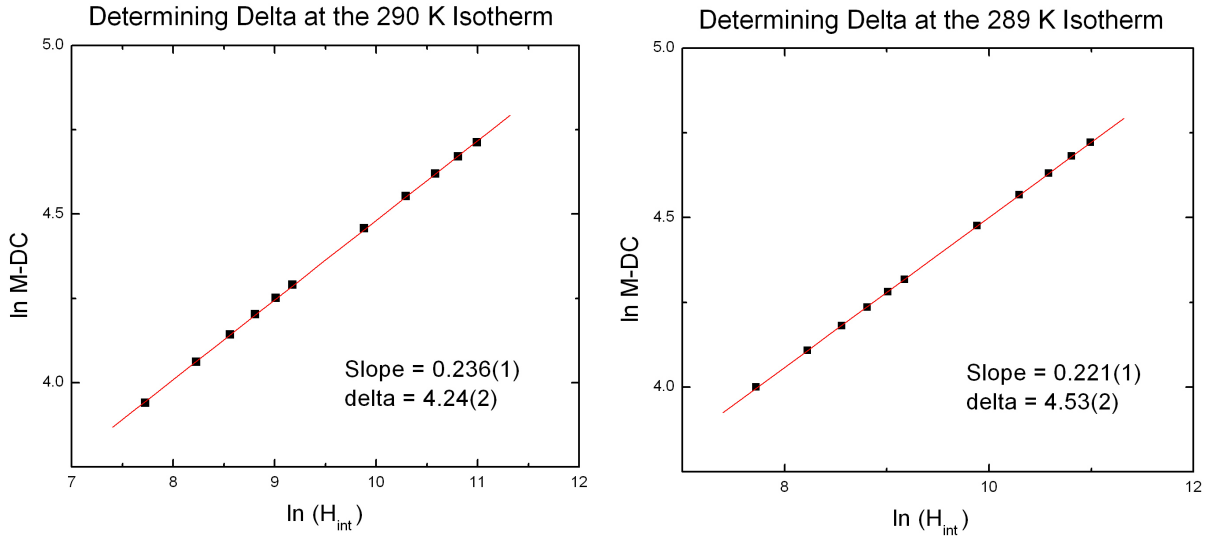

From the interpolation, $\delta = 4.32 \pm 0.02$. Now, critical exponents must obey the Widom scaling relation [25]

$$\delta = 1 + \gamma/\beta. \tag{17}$$

Inserting the experimental values for β and γ yields $\delta = 4.34 \pm 0.03$; thus, the Widom scaling relation is satisfied.

C. AC susceptibility

The data in Figure 6 shows how the ac susceptibility varies over the entire temperature range of the instrument. One can see that the susceptibility falls dramatically near 300 K (see inset in Figure 6). This is one indication that a ferromagnetic-paramagnetic transition is taking place.

Figure 6: AC susceptibility as a function of temperature (20 K ≤T ≤ 350 K)

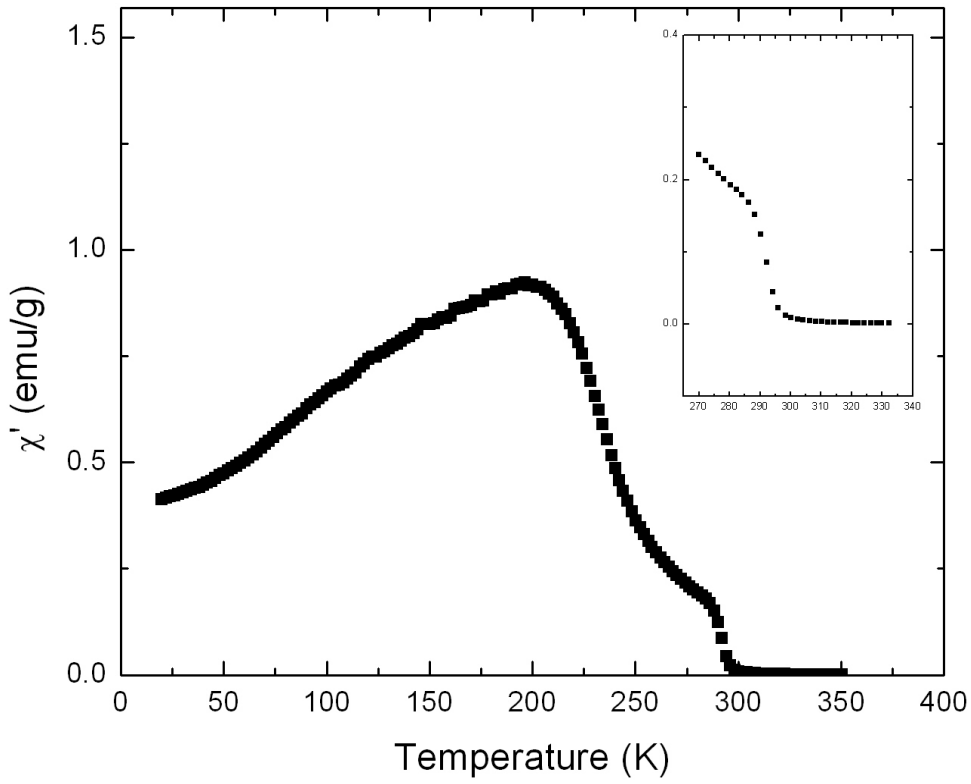

When a system undergoes a paramagnetic to ferromagnetic transition, the AC susceptibility as a function of temperature with a DC magnetic field superimposed has a peak near the transition temperature. This peak shifts with a change in the applied field, which is a signature of critical fluctuations that occur during a phase transition. The data in Figure 7 confirms that a phase transition is indeed taking place in the nanostructured Gd sample.

Figure 7: AC susceptibility vs Temperature with DC bias fields for temperatures near the transition temperature. Bias fields range from 600 Oe to 3000 Oe in intervals of 200 Oe. The red line on the graph passes through the T_m points and indicates how the peak is shifting to higher temperatures.

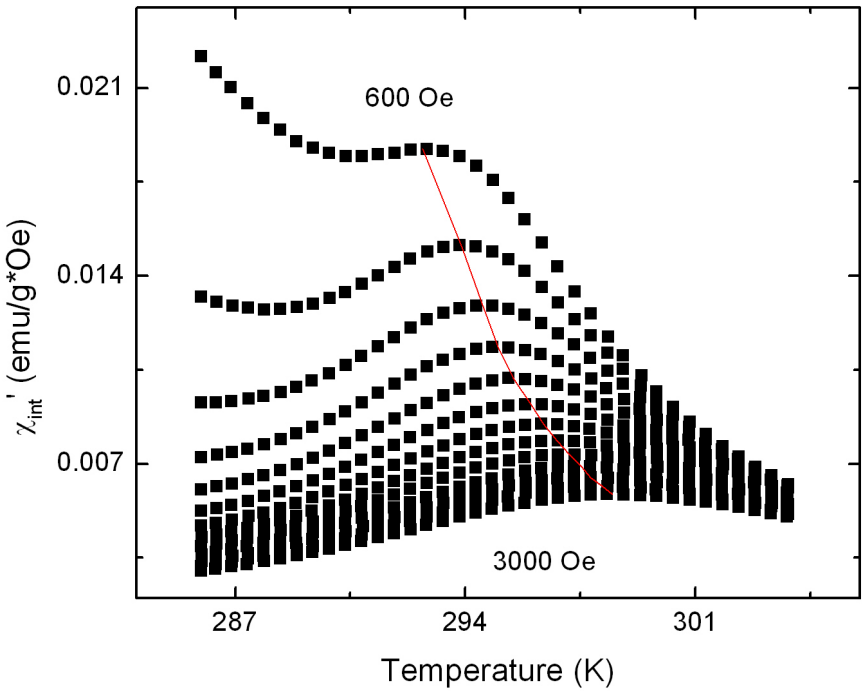

The maximum susceptibility was located on each data set, and the temperature at which that maximum occurs was recorded as T_m. At each T_m, $\varepsilon_m = (T_m - T_C)/ T_C$ was calculated. Now, as demonstrated earlier, $\varepsilon_m \propto H_i^{1/(\gamma+\beta)}$, from which we obtain:

$$T_m = (k * T_C)\left(H^{\frac{1}{\gamma+\beta}} \right) + T_C . \qquad (18)$$

The data in Figure 8 show that T_C using this relation is 290.2 ± 0.7 K, agreeing within uncertainty limits with the T_C from the DC magnetization data. The values for γ and β were taken from the best values obtained from the Arrott-Noakes analysis.

Figure 8: T_m versus $H^{(1/(\gamma+\beta))}$. The intercept on the vertical axis gives a measure of T_C.

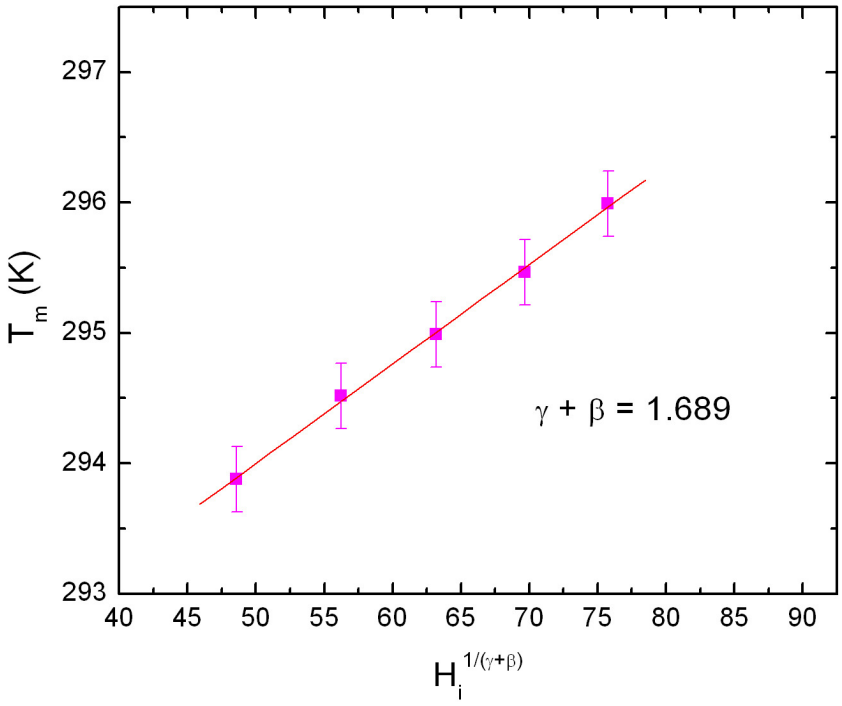

The AC susceptibility data can also be used to determine gamma. From the relation **(3)** it follows that follows that

$$\chi'(h,t) \propto \varepsilon_m^{-\gamma} \tag{19}$$

Plots of ln (χ') vs. the ln (ε_m) can thus provide a measurement of γ.

Figure 9: Log-Log plot of internal susceptibility vs reduced temperature, ε_m. γ is equal to the negative of the slope.

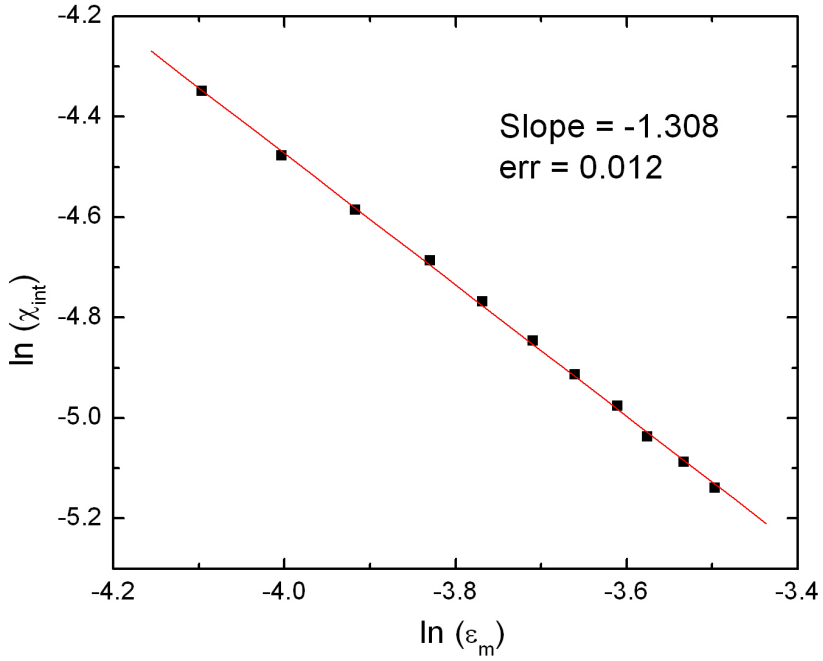

The data in Figure 9 is linear for applied fields greater than 1000 Oe, and its slope results in $\gamma = 1.308 \pm 0.012$.

II. $Gd_{94.6}Fe_{5.4}$

A. Structural Properties

The x-ray diffraction data shows the sample to be composed of nanocrystalline grains with diameters of approximately 70 nm. Also, the x-ray diffraction lacks peaks for Fe, indicating it is located in the noncrystalline regions of the sample. Energy-dispersive x-ray spectroscopy also indicates that the Fe concentration in the grain goes to zero, showing that the sample is composed of grains of pure Gd, with amorphous Gd and Fe present in the grain boundaries. TEM images confirm the sample's nanocrystalline grain structure. EXAFS data reveals that the volume of the sample occupied by the grains decreased in comparison to the pure Gd sample [24].

B. DC Magnetization

In order to facilitate a more robust analysis of the DC magnetization data, we took data at a smaller temperature intervals and higher applied field than the ms-Gd sample. Because we had more isotherms available for the $Gd_{54.6}Fe_{5.4}$ data, we were able to use numerical derivatives in the iterative KF process to determine the critical exponents of this sample. The code used to run the process is included as Appendix I. The process was run using a range of initial exponents, $\gamma = 1.15\text{-}1.45$ and $\beta = 0.36\text{-}0.42$. All initial values converged to the same critical exponent values within uncertainty.

Because the extrapolations to estimate M_s and χ_0^{-1} are only valid for sufficiently high values of H, some lower field data points were excluded from the linear extrapolations. We used the eight highest field values because the KF process converged in the fewest number of iterations.

The result of the KF process was a Tc = 291.710±0.07, γ = 1.2438(1), and β = 0.385(1). The AN plot for these exponents is below in figure 10.

Figure 10: AN plot for $Gd_{94.6}Fe_{5.4}$ sample

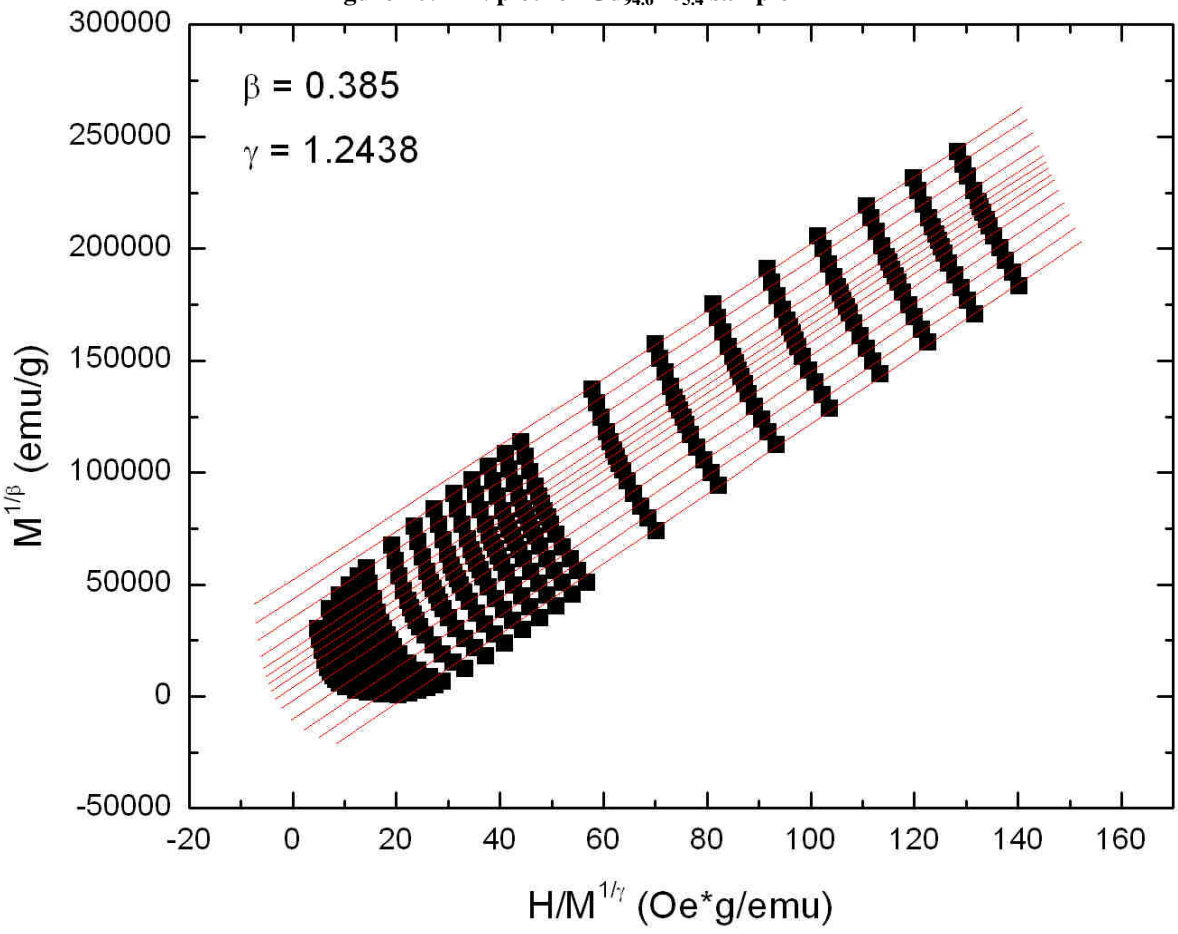

We can use the single power laws to check these values for the exponents. We use the extrapolations from the final AN plot to get M_s and χ_0^{-1}, and then use the non-linear curve fitting routine to fit the data to the SPL in **(2)** and **(3)**. Allowing T_c, the exponent, and the critical amplitude to vary freely, we can check the KF method. The fitting is displayed in figure 11.

Figure 11: Results for SPL fitting for Gd94.6Fe5.4 The squares are the data, and the line is the fitting results. The top graph determines β and B and the bottom determines γ and Γ.

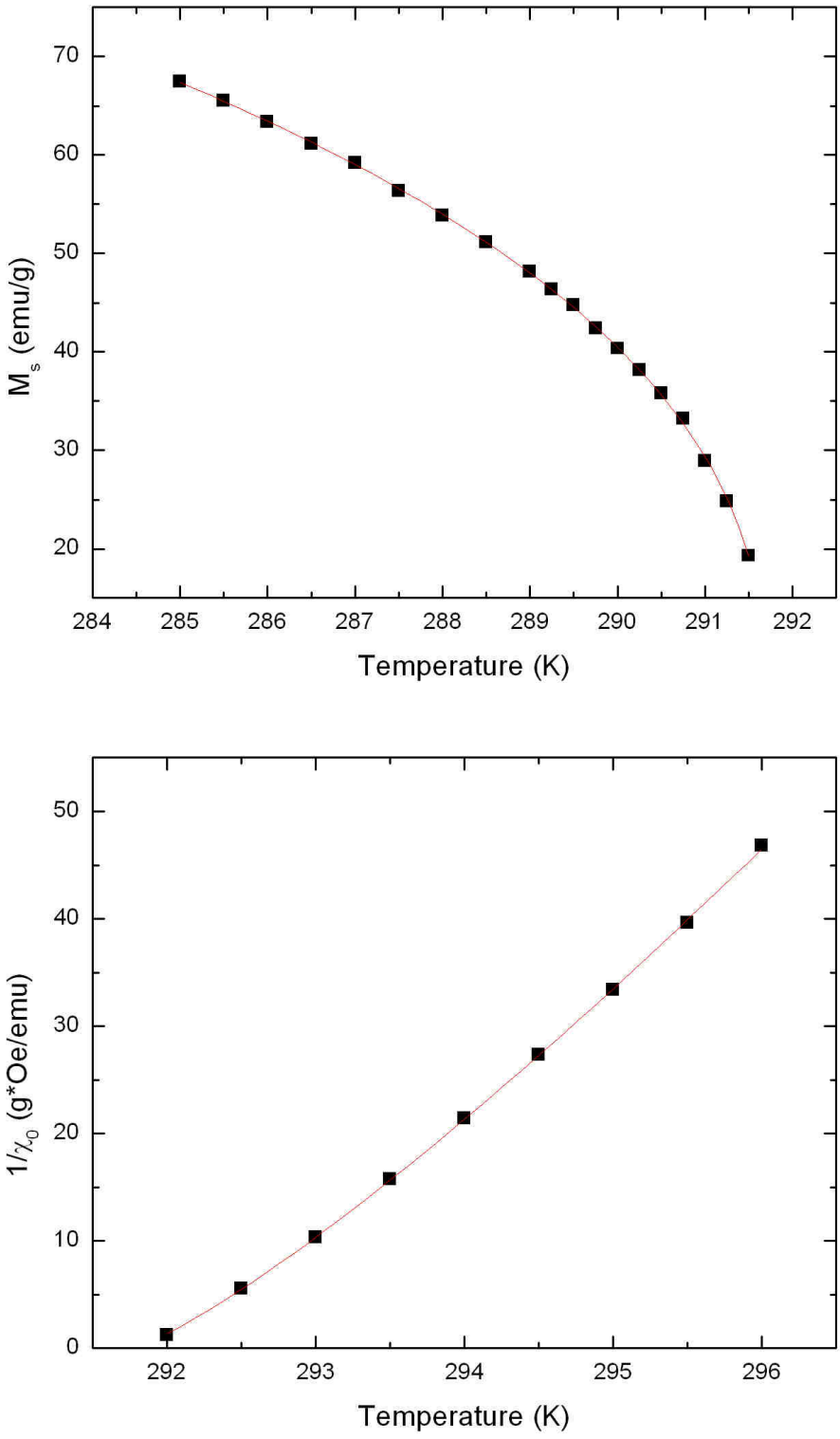

Single power law fits yield $\gamma = 1.22 \pm 0.05$, $\beta = 0.376 \pm 0.004$, and $T_c = 291.76 \pm 0.1$ and 291.73 ± 0.05 for γ and β respectively, so the SPL fits agree with the KF method within uncertainty. The SPL fitting also found the critical amplitude M_0 to be 278 ± 4 and the critical amplitude $(h_0/M_0) = \Gamma_0$ to be 8140 ± 1000.

With T_c known, we can make a measure of delta from the magnetization data. From the single power law in equation **(4)**, we can estimate delta from the slope of a log-log plot of magnetization versus internal field. Since we did not have data for an isotherm exactly at T_c, we found an effective delta for the two isotherms closest to T_c and linear interpolated to find delta. The result was a value of 4.2006 ± 0.04 for delta. The Widom scaling relation is satisfied for this value, as $1 + \gamma/\beta$ is 4.22.

We can gain more insight in to the transition by observing how the exponents vary near the phase transition. The graphs in figures 12 and 13 use the single power laws in a rearranged form similar to the intercept method. But instead of just looking that the overall slope to determine a single value for the exponent, we take a numerical derivative to study the slope, which is the value of the exponent, at each data point, allowing us to observe trends as the sample approaches the transition. In this case, the exponents stay reasonably constant throughout the transition. The larger graphs contain the raw data, and the insets are derivatives. To take the numerical derivatives, the raw data was interpolated using a cubic spline, and then differentiated. The data points in the inset then are the values of the smoothed derivative at the temperature points of the raw data.

Figure 12: The slope of the log-log plot of reduced temperature vs spontaneous magnetization gives the value of the critical exponent β. The inset shows the derivative of the graph (β_{eff}) vs reduced temperature, revealing how the exponent varies as the reduced temperature is changed.

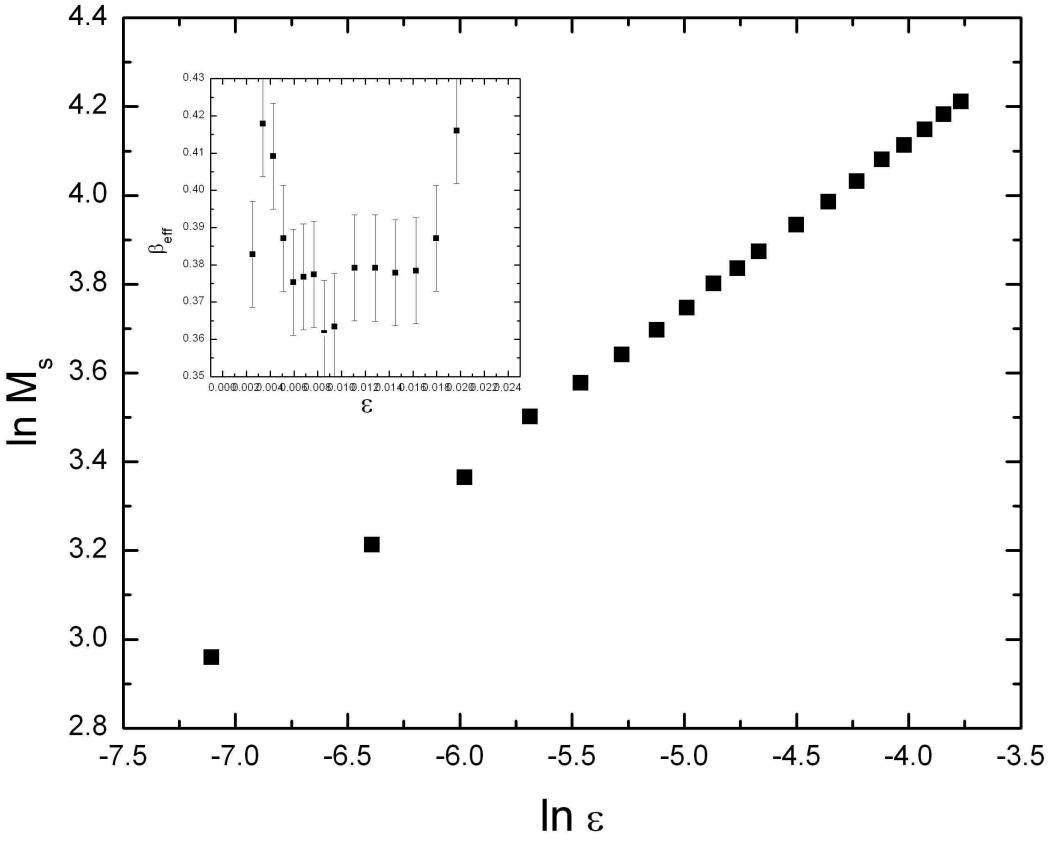

Figure 13: The slope of the log-log plot of reduced temperature vs the inverse of the zero field susceptibility gives the value of the critical exponent γ. The inset shows the derivative of the graph (γ_{eff}) vs reduced temperature, revealing how the exponent varies as the reduced temperature is changed.

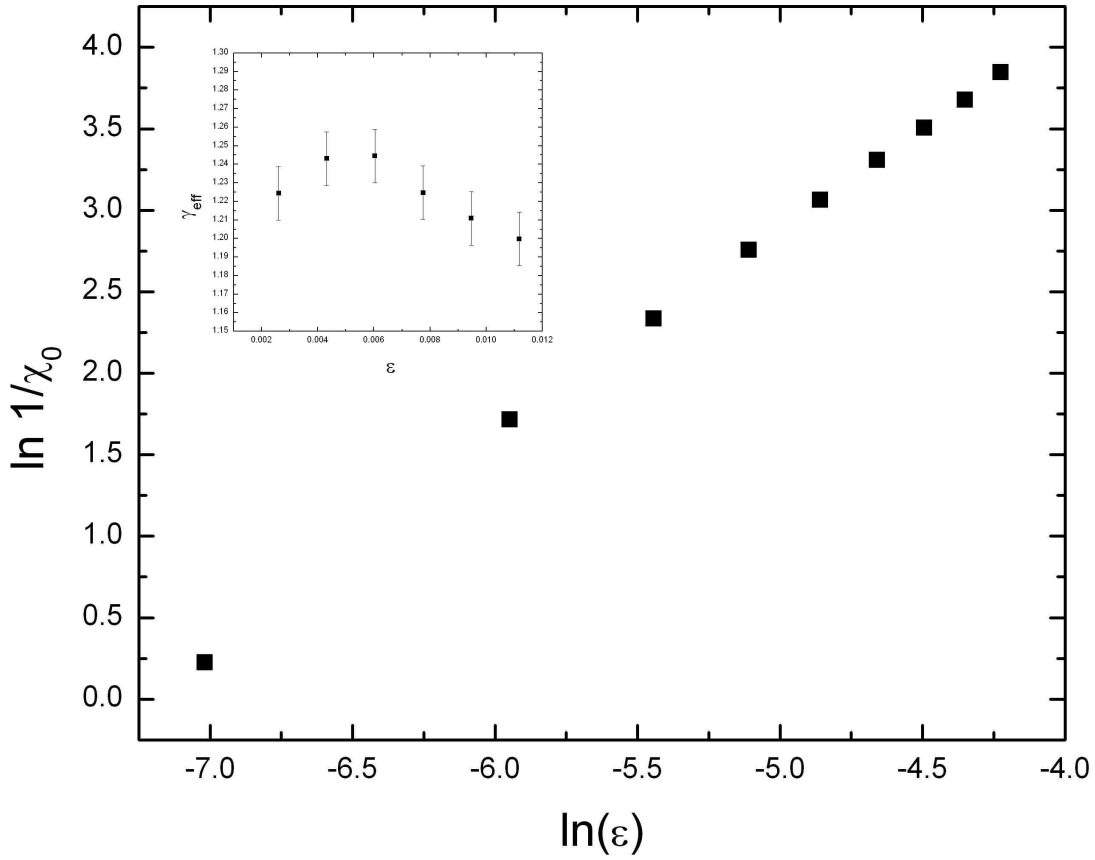

A final technique we created for studying the critical exponents of the sample was what we call the exponent map method. In this technique, we used a computer program to perform one KF iteration for a wide variety of initial γ and β values and compared the updated exponents with the initial values. The program can be found in Appendix II. The value of the difference was plotted as a height over an x-y axis, with the x-axis representing the initial values of γ and the y-axis representing the initial value of β. Since the KF method is considered complete when the initial and updated exponents are constant, any where on this surface with a height of zero should be a likely value for an exponent. For $Gd_{94.6}Fe_{5.4}$, the exponent map corroborates the results

from the KF method. The exponent maps can be seen in figures 14 and 15 where the color represents the difference.

Figure 14: Exponent Map method for the β value

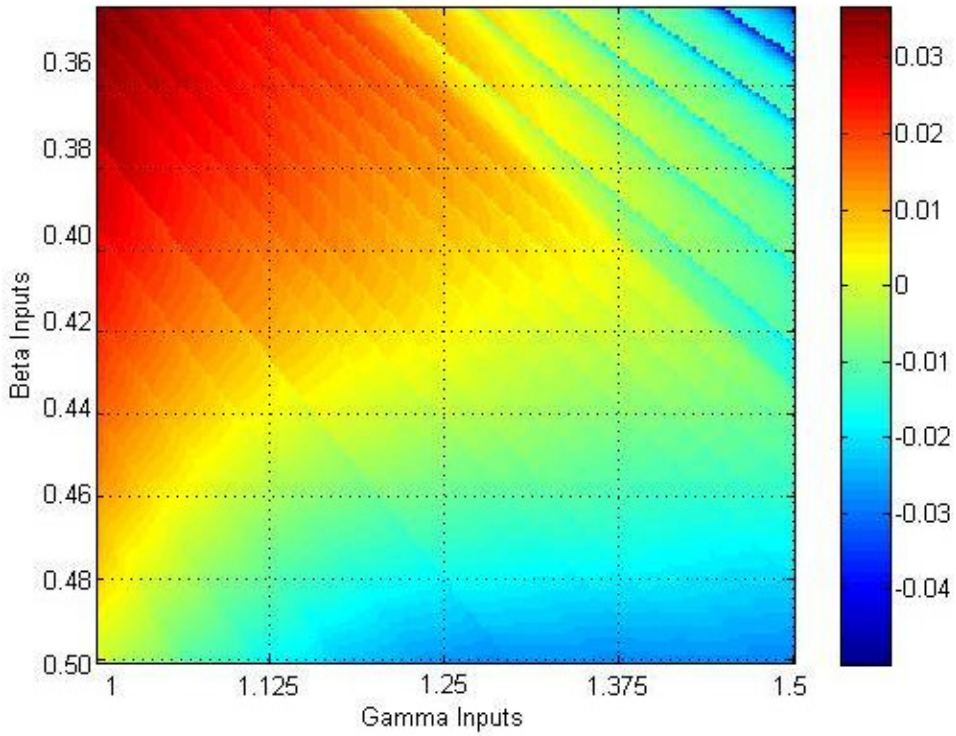

Figure 15: Exponent Map Method for γ value

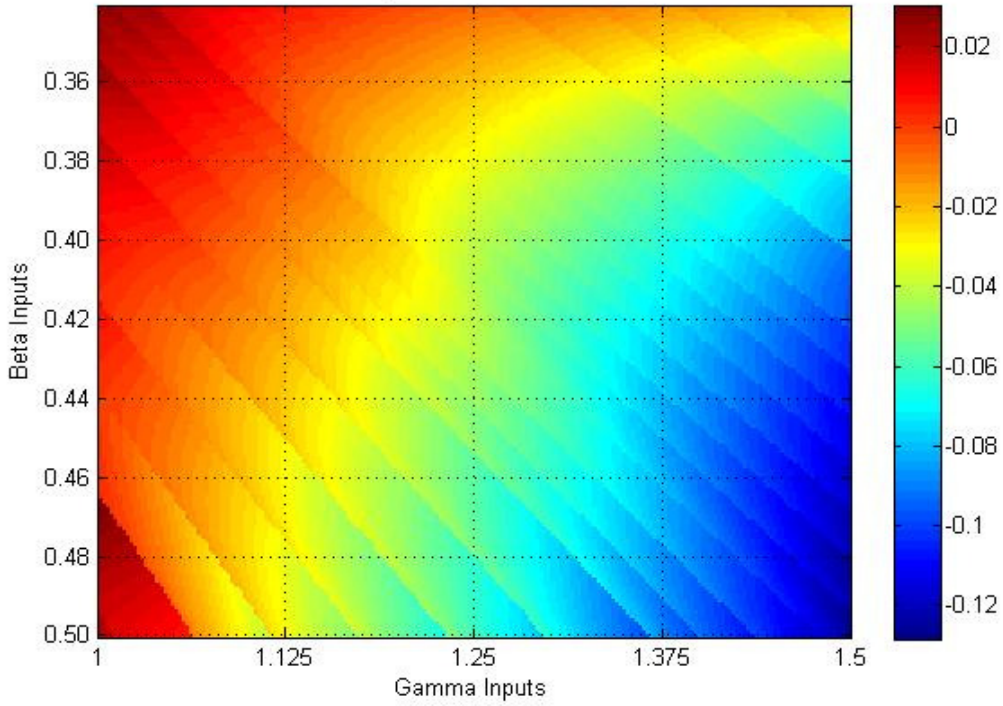

III. $Gd_{97}Fe_3$ and $Gd_{80}Fe_{20}$

A. Structural Properties

The structural analysis of samples containing 3% Fe and 20% Fe showed that the grain size of the samples were similar to that of the pure Gd and $Gd_{94.6}Fe_{5.4}$, approximately 70 nm. The volume of the grain boundaries increased with an increase in Fe content across all samples tested. Energy-dispersive x-ray spectroscopy indicates that the Fe remains in the grain boundary region [24].

B. DC Magnetization

The magnetization versus applied field data for both samples are shown in figures 15 and 16. In proceeding with the KF method described earlier, we were unsuccessful in determining critical exponents from the data for these two samples. As the KF method would progress, the calculated T_c would continue to rise beyond what AC susceptibility measurements indicated was the transition temperature. For the $Gd_{97}Fe_3$ sample, there was one set of exponents on which the KF method would converge; however, the isotherms in the AN plot still had a significant curvature, as seen in figure 17. At this time, we are not able to resolve this problem and arrive at values for the critical exponents that describe the system.

Figure 15: Magnetization vs external field data for $Gd_{97}Fe_3$. Data was taken at such small intervals that the the data points overlap.

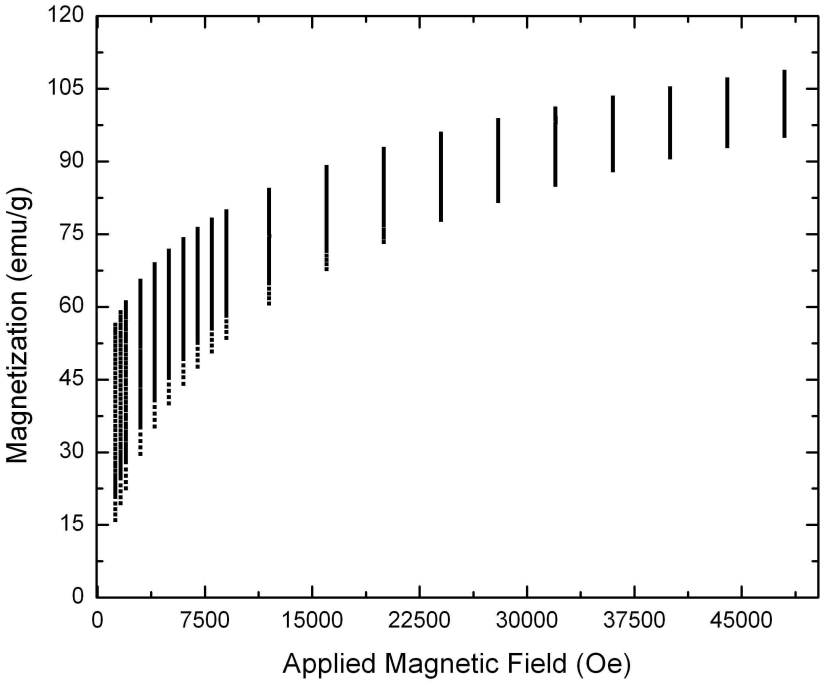

Figure 16: Magnetization vs external field data for $Gd_{80}Fe_{20}$.

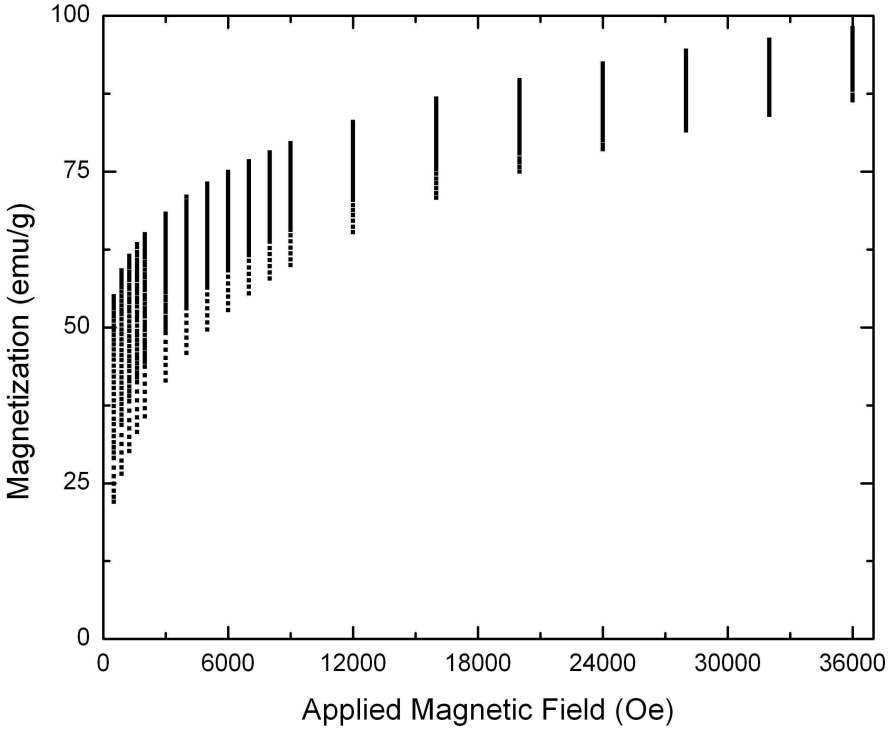

Figure 17: AN plot for the critical exponents that resulted from the KF method for $Gd_{97}Fe_3$. Not that the isotherms are not linear.

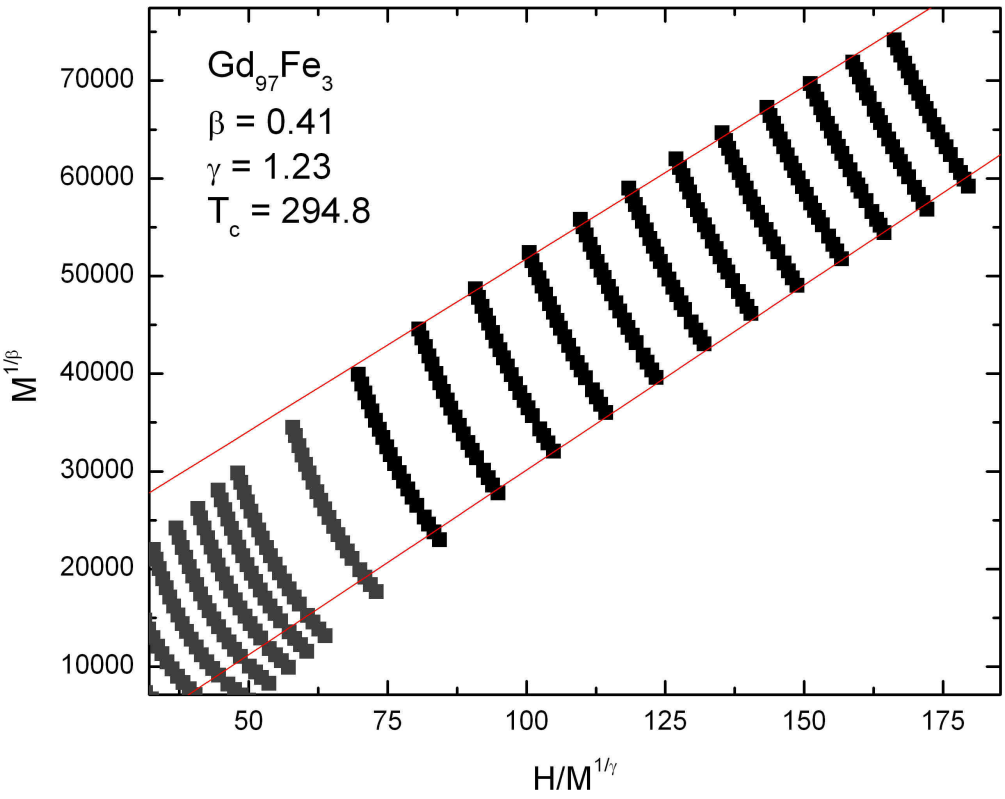

Discussion:

The critical-exponent values for melt-spun gadolinium, melt-spun $Gd_{100-x}Fe_x$, bulk crystalline gadolinium, and other amorphous gadolinium based ferromagnets, as well as some theoretical values for the exponents, are included in Table 2 for comparison.

Table 2: Comparisons of parameters of pure ms-Gd sample with experimental and theoretical values report in literature.

Material	Ref.	β	γ	δ	T_C (K)
Ms-Gd	This work	0.389 ± 0.017,	1.300 ± 0.014,	4.32 ± 0.02	289.70 ± 0.1
Ms-$Gd_{94.6}Fe_{5.4}$	This work	0.385 ± 0.001	1.243 ± 0.001	4.20 ± 0.02	291.71 ± 0.1
Crystalline Gd (Isotopic Dipolar Regime)	[12]	0.40±0.02	1.39±0.03		292.78±0.01
Crystalline Gd (Uniaxial Regime)	[12]	0.5002±0.0006	1.00±0.03	3.005(5)	292.78±0.01
Amorphous Gd-TM Ferromagnets	[19]	0.34 – 0.44	1.16 – 1.29	3.6 – 3.96	--
3D Heisenberg Model (Theory)	[19]	0.365(25)	1.386(4)	4.80(4)	--
Mean Field Theory	[25]	0.5	1	3	--

The critical temperature of ms-Gd is approximately 4 K lower than that of bulk Gd, and approximately 1.5 K lower than polycrystalline samples [19]. This leads us to conclude that the nanocrystallinity of the sample is resulting in a depression of the transition temperature. M. Tokita et al. have shown that applying pressure to bulk gadolinium depresses the transition temperature [10]. Michels, Krill, and Birringer apply this to their nanocrystalline sample of Gd, positing that each grain is having pressure applied by the amorphous grain boundary regions [9]. For grain sizes from 10 nm to 100nm, they determined an empirical relationship between the grain size and the reduction in T_c: $-\Delta T_c \propto D^b$, with $b \approx -1$. Using this relation, a shift in T_c of about 4 K would be expected for the average grain size in ms-Gd, which corroborates the T_c found experimentally. We conclude that the grain boundary regions are applying a pressure to

the crystalline grains present in the sample, leading to the lowering of the transition temperature of the nanocrystals, and thus lowering the bulk material's critical temperature.

The transition temperature for the ms-$Gd_{94.6}Fe_{5.4}$ sample is still depressed relative to the bulk, although not as much as in the pure ms-Gd sample. Because structural analysis reveals that the nanocrystalline grains are essentially still pure Gd , the addition of the Fe does not change the characteristics of the grains themselves. One explanation for the observed reduction of T_c is that the Fe collecting in the grain boundaries is changing the structure of the boundaries and having an effect on the pressure exerted. However, we cannot make a conclusion with only one mixed sample.

Because ms-Gd is essentially composed of a large number of nanocrystals that would essentially behave as small bulk samples, we expect that the critical exponents of the phase transition would not be significantly affected. The experimentally determined value of $\beta = 0.389 \pm 0.017$ compares well with the value determined by Srinath and Kaul (SK) [12]. The value for γ (1.39±0.03) obtained by SK seems to disagree with the value we have found for ms-Gd. However, SK has also shown that the value for γ is not constant throughout the entire range of reduced temperature ε. The gadolinium system goes through a crossover from the isotropic universality class ($\gamma = 1.386$) to uniaxial dipolar universality class ($\gamma = 1$) as the transition temperature is approached. These crossovers are reflected in the changing value of γ as T_c is approached. In SK's determination of γ, a reduced temperature range of $2.0\times10^{-3} \le \varepsilon \le 6.8\times10^{-3}$ was used [12]. Our reduced temperature range encompasses both SK's range and the low end of the reduced temperature range not included by SK where γ rapidly falls to a mean field value of 1. Thus, it is not surprising that we measured a smaller value of γ.

Ms-$Gd_{94.6}Fe_{5.4}$ also has a value of β that compares well with the value for monocrystalline Gd. However, the value of γ has moved away from the asymptotic critical value of monocrystalline Gd even more. The reduced temperature range for this sample is $8.7\times10^{-4} \le \varepsilon \le 1.46\times10^{-2}$. Thus, it is possible that the lowering of the critical exponent comes from including data from the region where γ decreases to 1 as it changes universality class. However, the data in figure 13 indicate that the exponent is approximately constant throughout the range of reduced temperature. The fact that the effective value of the critical exponent remains constant in the reduced temperature range indicates that the value of the exponent is an asymptotic value. This argument is further supported by the inability of the correction-to-scaling expansion to improve the fits in figure 11. If the data was outside of the asymptotic region, the difference could be compensated for using the CTS expansion, but since the fit does not improve with the extra terms, there is no difference for the CTS to take into account. The value of the exponent is in between the isotropic dipolar value and the mean-field value, possibly because the sharp transition between the two universality classes present in ms-Gd has become smeared out due to the disorder in the grain boundaries.

Another possibility is that the iron is actually changing the asymptotic critical exponent by effectively reducing that material's spatial dimensionality. A material's dimensionality governs how many nearest neighbors it can interact with. Because the interactions with nearest neighbors are vital to a PM-FM phase transition, different dimensionality classes result in very different theoretical critical exponents. For example, the critical exponent γ in the 3-D Ising Model is predicted to be 1.238, but in the 2-D Ising model, it is predicted to be 1.75. Beauvillain et al. hypothesized for a sample of $LiTbF_4$ that showed mean field-like γ values, but changed to a γ value of 1.215 after being diluted with Yttrium, that the Yttrium could be effectively changing

the dimensionality [27]. Gd also changes from uniaxial dipolar universality class ($\gamma = 1$) to a higher asymptotic γ value as iron is introduced into the system. Thus, it may be that iron is effectively reducing the dimensionality in the sample. In order to draw more conclusions about the effects of iron on the PM-FM transition, more samples containing different amounts of iron must be analyzed.

Unfortunately, we were unsuccessful in applying standard KF analysis to the $Gd_{97}Fe_3$ and $Gd_{80}Fe_{20}$ samples in the time available. When the KF analysis is applied, the transition temperature measured is higher than expected in comparison with other samples and ac susceptibility data. This leads us to hypothesize that Fe, which is ferromagnetic at temperatures in the vicinity of the Gd T_c, is initiating a non-zero magnetization above the Gd PM-FM transition. Since the KF method assumes a sharp transition, this non-zero magnetization may be causing the KF method to fail. One possible method of examining the transition is to determine the contribution of the Fe to the magnetization and subtract it from the measurement, allowing us to perform KF analysis on the Gd magnetization only. As research moves forward, this method, in addition to other approaches, will be employed to determine the critical exponents of these composite systems.

Conclusion:

Melt-spun Gd and GdFe alloy ribbons are comprised of many nanocrystalline grains of pure Gd that are embedded in an amorphous grain boundary phase. This two-phase structure affects the paramagnetic to ferromagnetic transition primarily through a mechanism where extra pressure is applied to the Gd grains and the T_c is lowered.

Through the use of the "intercept method," the critical exponents for the ms-Gd system were determined to be similar to that of monocrystalline Gd when the crossover effects were taken into account. This indicates that the phase transition behavior of nanocrystalline Gd is comparable to monocrystalline Gd. Though our analysis of ms-Gd was somewhat limited by not having enough isotherms as needed to reliably perform KF or SPL analysis, we were still able to obtain robust measurements of the critical exponents, T_c, and the critical amplitudes by using the ac susceptibility data and scaling analysis.

For the ms-$Gd_{94.6}Fe_{5.4}$ sample, we increased the amount of data taken so that we could expand our analysis of DC magnetization. Adding iron to the system appears to increase the volume fraction of the grain boundary regions while not affecting the grain size. This change in the grain boundaries could affect the pressure on the grains and account for the change in the transition temperature. The asymptotic value of the critical exponent gamma is significantly different from the ms-Gd sample, possibly indicating that iron in the grain boundaries is effectively changing the dimensionality of the Gd grains.

The data from the ms-$Gd_{97}Fe_3$ and ms-$Gd_{80}Fe_{20}$ samples could not be analyzed using conventional KF analysis. Iron in the sample appears to lead to a nonzero magnetization above the transition temperature, complicating the transition made by the Gd grains. Ascertaining the

affects of adding Fe to the ms-Gd system will continue by examining the component of the magnetization due to iron and studying more samples of varying compositions.

In addition to quantifying the effects of nanoscale disorder introduced by melt-spinning, this study has tested and compared various methods of analyzing nanostructured samples, including scaling analysis, KF method, and SPL fitting. Furthermore, routines have been developed so that similar measurements in the future can be quickly investigated in a way consistent with previous analysis methods.

Literature Cited:

[1] http://nobelprize.org/nobel_prizes/physics/laureates/2007/index.html

[2] A. P. Ramirez. *Colossal magnetoresistance*. J. Phys.: Condens. Matter 9 (1997) 8171-8199.

[3]Cui, Yi. Science 291 (2001) 851-853.

[4] QA Pankhurst, J Connolly, SK Jones, J Dobson. Applications of Magnetic Nanoparticles in Biomedicine. J. Phys. D: Appl. Phys 36 (2003) R167-R181.

[5] M. A. Morales, D. S. Williams, P. M. Shand, C. Stark, T. M. Pekarek, L. P. Yue1, V. Petkov, and D. L. Leslie-Pelecky. *Disorder-induced depression of the Curie temperature in mechanically milled* $GdAl_2$. Phys. Rev. B 70, (2004) 184407.

[6] R. Kruk, M. Ghafari, H. Hahn, D. Michels, R. Birringer, C. E. Krill III, R. Kmiec, M. Marzalek. Phys. Rev. B 73 (2006) 54420.

[7] H. E. Nigh, S. Legvold, F. H. Spedding. Phys. Rev. 132, (1963) 1092 – 1097.

with critical exponents are $\gamma = 1.196$, $\beta = 0.381$, and $\delta = 3.615$ [14].

[8] S. Yu. Dan'kov, A. M. Tishin, V. K. Pecharsky, and K. A. Gschneidner Jr. Phys. Rev. B. 57 (1998) 3478-3490.

[9] D. Michels, C.E. Krill III, and R. Birringer. J. Magn.Magn. Mater. 250 (2002) 203.

[10] M. Tokita, K. Zenyo, H. Kubo, K. Takeda, M. Mito, T. Iwamoto. J. Magn. Magn. Mater. 272 (2004) 593.

[11] Wang Dun-hui, Han Zhi-da, Huang Song-ling, Peng Kun, Wang Yi, Zou Wen-qin, Gu Ben-xi, Du Yo-wei. Physica B 352 (2004) 185.

[12] S. Srinath, S. N. Kaul. Phys. Rev. B. 60 (1999) 12166 – 12176.

[13] K. Yano,Y. Akiyama, K. Tokumitsu, E. Kita, and H. Ino. J. Magn. Magn. Mater. 214 (2000) 217-224.

[14] V. Petkov, K. Yano, E. Kita. Phys. Stat. Sol. 157 (1996) 365-372.

[15] C. M. Hurd, Contemp. Phys. 23 (1982) 469-493.

[16] S. Blundell. *Magnetism in Condensed Matter.* (Oxford Press, 2001).

[17]Amra Peles, M.S. thesis, University of Manitoba, 1999.

[18] M. Sahana, U.K. Röβler, N. Ghosh, S. Elizabeth, H.L. Bhat, K. Dorr, D. Eckert, M. Wolf, K.H. Müller. Phys. Rev. B. 68 (2003) 144408.

[19] S. N. Kaul. J. Magn. Magn. Mater. 53 (1985) 5-53.

[20] A. Arrott, J. Noakes. Phys. Rev. Lett. 19 (1967) 786-789.

[21] J. Kouvel, M. Fisher. Phys. Rev. 136 (1964) A1626 - A1632.

[22] S.F. Fischer, S.N. Kaul, and H. Kronmueller. Phys. Rev. B. 65 (2002) 064443-1-12.

[23] J.H. Zhao, H.P. Kunkel, X.Z. Zhou, G. Williams, M.A. Subramanian. Phys. Rev. Lett. 83 (1999) 219-222.

[24] Schmitter, D. *Correlating Disorder and Magnetism in Gadolinium and Gadolinium-iron Nanostructures*. PhD thesis, University of Nebraska-Lincoln (2007).

[25] M. Plischke, B. Bergersen. *Equilibrium Statistical Physics*, 2nd Ed. (1994) Singapore: World Scientific Publishing Co.

[26] S. Dan'kov, A. M. Tishin, V. K. Pecharsky, K. A. Gschneidner Jr. Phys. Rev. B 57 (1998) 3478-3490.

[27] P. Beauvillain, C. Chappert, J. P. Renard, J. A. Griffin. J. Phys. C: Sol St. Phys. 13 (1980) 395-402.

Appendix I:

```
%ECPGdFe54_newdata_iterativemethod
%Get Inputs
clear diff_tc Results
close all

Tuse = 28;
Fieldponts = 22;

 t2=0;
 for betaloop = 1:7

     for gammaloop = 1:5
 t2=t2+1;

t=0;
Betain = 0.36 + (betaloop-1)*0.01;
Gammain = 1.15 +(gammaloop-1)*0.05;
Beta_new = Betain;
Gamma_new = Gammain;
Beta_out_KF = 0;
Gamma_out_KF = 0;
Results(t2,1) = Betain;
Results(t2,2) = Gammain;


while ((abs(Betain-Beta_out_KF)>0.0001)||(abs(Gammain-Gamma_out_KF)>0.0001))
    t = t+1;
    if t>400
        break;
    end
    Betain = Beta_new;
    Gammain = Gamma_new;

clear RawData2 BetaData BetaDataLength GammaData GammaDataLength der der2 d
extra p Betalnt_m Gammalnt_m Tc_intercept lnt_m spon_mag Gamma_out_Intercept
Beta_out_Intercept;
for j=1:Tuse
    RawData2(1:22,(j*2)-1) = RawData1(1:22,(j*2)-1).^(1/Gammain);
    RawData2(1:22,(j*2)) = RawData1(1:22,j*2).^(1/Betain);
    p = polyfit(RawData2(15:22,(j*2)-1),RawData2(15:22,(j*2)), 1);
    Data(j,2) = p(2);
    Data(j,3) = p(1);
end

%Intecept Method
%calculate tc from the y-int vs Temp y-intercept
p = polyfit(Data(1:Tuse,1), Data(1:Tuse,2), 1);
Tc_intercept = -p(2)/p(1);

%Get the correct data for the different exponents
for j=1:Tuse
    if Data(j,2)>0
```

```
    BetaData(j,1) = Data(j,1);
    BetaData(j,2) = Data(j,2);
    BetaData(j,3) = Data(j,3);
    end
end
d=size(BetaData);
BetaDataLength = d(1);

extra = 0;
for j=1:Tuse
    if Data(j,2)<0
    GammaData(j-extra,1) = Data(j,1);
    GammaData(j-extra,2) = Data(j,2);
    GammaData(j-extra,3) = Data(j,3);
    GammaData(j-extra,4) = -Data(j,2)/Data(j,3);
    else
    extra = extra+1;
    end
end
d=size(GammaData);
GammaDataLength = d(1);

%t_m reduced temperature
Betalnt_m = log(abs((Tc_intercept-
BetaData(1:BetaDataLength,1))/Tc_intercept));
Gammalnt_m = log(abs((Tc_intercept-
GammaData(1:GammaDataLength,1))/Tc_intercept));

%get spontaneous magnetization
spon_mag = BetaData(1:BetaDataLength,2).^Betain;
lnspon_mag = log(spon_mag);

%get log(1/X)
chi_inverse = GammaData(1:GammaDataLength,4).^Gammain;
lnchi_inverse = abs(log(chi_inverse));

p=polyfit(Gammalnt_m, lnchi_inverse, 1);
Gamma_out_Intercept = p(1);
p=polyfit(Betalnt_m, lnspon_mag, 1);
Beta_out_Intercept = p(1);



%Kouvel-fisher

%Derivative of spon_magnetization

der(1,1) = (spon_mag(2)-spon_mag(1))/(Data(2,1)-Data(1,1));
for j=2:(BetaDataLength-1)
    der(j,1) = (spon_mag(j+1)-spon_mag(j-1))/((Data(j+1,1)-Data(j-1,1)));
end
der(BetaDataLength,1) = (spon_mag(BetaDataLength)-spon_mag(BetaDataLength-
1))/(Data(BetaDataLength,1)-Data(BetaDataLength-1,1));

%Divide the derivative by the spontaneous magnetization, then do a linear fit
```

```
M_s_derM_s = spon_mag./der;
p = polyfit(Data(2:BetaDataLength-1,1),M_s_derM_s(2:BetaDataLength-1),1);
Beta_out_KF = 1/p(1);
Beta_new = Beta_out_KF;
Tc_beta_KF = abs(p(2)/p(1));


%Derivative of 1/X

der2(1,1) = (chi_inverse(2)-chi_inverse(1))/(Data(2+extra,1)-
Data(1+extra,1));
for j=2:(GammaDataLength-1)
    der2(j,1) = (chi_inverse(j+1)-chi_inverse(j-1))/((Data(j+1+extra,1)-
Data(j-1+extra,1)));
end
der2(GammaDataLength,1) = (chi_inverse(GammaDataLength)-
chi_inverse(GammaDataLength-1))/(Data(GammaDataLength+extra,1)-
Data(GammaDataLength-1+extra,1));

%Divide the derivative by the spontaneous magnetization, then do a linear fit
c_i_derc_i = chi_inverse./der2;
p = polyfit(GammaData(2:GammaDataLength-1,1),c_i_derc_i(2:GammaDataLength-
1),1);
Gamma_out_KF = 1/p(1);
Gamma_new = Gamma_out_KF;
Tc_Gamma_KF = abs(p(2)/p(1));



Results(t2,3) = Beta_out_KF;
Results(t2,4) = Gamma_out_KF;
Results(t2,5) = Tc_Gamma_KF;
Results(t2,6) = t;


end

    end
end

hold on
for j=1:Tuse
plot(RawData2(1:Fieldponts,(j*2)-1),RawData2(1:Fieldponts,(j*2)),'o');
end
str1 = num2str(Gamma_new);
str2 = num2str(Beta_new);
title('Arrott-Noakes Plot')
text(10,300,str1,'Units','pixels');
text(10,250,str2,'Units','pixels');
text(10,200,num2str(Tc_Gamma_KF),'Units','pixels');
xlabel('H/M^1^/^y')
ylabel('M^1^/^B')
hold off
```

Appendix II:

```
%Get Inputs
clear diff_tc

for b = 1:40
    Betain = 0.35 + b*0.002;
     diff_tc(b+1,1) = Betain;
     gamma_inter(b+1, 1) = Betain;
     beta_inter(b+1, 1) = Betain;
     gamma_kf(b+1, 1) = Betain;
     beta_kf(b+1, 1) = Betain;
   for g = 1:45
       Gammain = 1.20 + g*0.005;
    diff_tc(1,g+1) = Gammain;
     gamma_inter(1,g+1) =Gammain;
     beta_inter(1,g+1) = Gammain;
     gamma_kf(1,g+1) = Gammain;
     beta_kf(1,g+1) = Gammain;

clear RawData2 BetaData BetaDataLength GammaData GammaDataLength der der2 d
extra p Betalnt_m Gammalnt_m Tc_intercept lnt_m spon_mag Gamma_out_Intercept
Beta_out_Intercept;
for j=1:27
    RawData2(1:11,(j*2)-1) = RawData1(1:11,(j*2)-1).^(1/Gammain);
    RawData2(1:11,(j*2)) = RawData1(1:11,j*2).^(1/Betain);
    p = polyfit(RawData2(1:11,(j*2)-1),RawData2(1:11,(j*2)), 1);
    Data(j,2) = p(2);
    Data(j,3) = p(1);
end

%Intecept Method
%calculate tc from the y-int vs Temp y-intercept
p = polyfit(Data(1:27,1), Data(1:27,2), 1);
Tc_intercept = -p(2)/p(1);

%Get the correct data for the different exponents
for j=1:27
    if Data(j,2)>0
    BetaData(j,1) = Data(j,1);
    BetaData(j,2) = Data(j,2);
    BetaData(j,3) = Data(j,3);
    end
end
d=size(BetaData);
BetaDataLength = d(1);

extra = 0;
for j=1:27
    if Data(j,2)<0
    GammaData(j-extra,1) = Data(j,1);
    GammaData(j-extra,2) = Data(j,2);
    GammaData(j-extra,3) = Data(j,3);
    GammaData(j-extra,4) = -Data(j,2)/Data(j,3);
    else
```

```
    extra = extra+1;
    end
end
d=size(GammaData);
GammaDataLength = d(1);

%t_m reduced temperature
Betalnt_m = log(abs((Tc_intercept-
BetaData(1:BetaDataLength,1))/Tc_intercept));
Gammalnt_m = log(abs((Tc_intercept-
GammaData(1:GammaDataLength,1))/Tc_intercept));

%get spontaneous magnetization
spon_mag = BetaData(1:BetaDataLength,2).^Betain;
lnspon_mag = log(spon_mag);

%get log(1/X)
chi_inverse = GammaData(1:GammaDataLength,4).^Gammain;
lnchi_inverse = abs(log(chi_inverse));

p=polyfit(Gammalnt_m, lnchi_inverse, 1);
Gamma_out_Intercept = p(1);
p=polyfit(Betalnt_m, lnspon_mag, 1);
Beta_out_Intercept = p(1);



%Kouvel-fisher

%Derivative of spon_magnetization

der(1,1) = (spon_mag(2)-spon_mag(1))/(Data(2,1)-Data(1,1));
for j=2:(BetaDataLength-1)
    der(j,1) = (spon_mag(j+1)-spon_mag(j-1))/((Data(j+1,1)-Data(j-1,1)));
end
der(BetaDataLength,1) = (spon_mag(BetaDataLength)-spon_mag(BetaDataLength-
1))/(Data(BetaDataLength,1)-Data(BetaDataLength-1,1));

%Divide the derivative by the spontaneous magnetization, then do a linear fit
M_s_derM_s = spon_mag./der;
p = polyfit(Data(1:BetaDataLength,1),M_s_derM_s(1:BetaDataLength),1);
Beta_out_KF = 1/p(1);
Tc_beta_KF = abs(p(2)/p(1));


%Derivative of 1/X

der2(1,1) = (chi_inverse(2)-chi_inverse(1))/(Data(2+extra,1)-
Data(1+extra,1));
for j=2:(GammaDataLength-1)
    der2(j,1) = (chi_inverse(j+1)-chi_inverse(j-1))/((Data(j+1+extra,1)-
Data(j-1+extra,1)));
end
```

```
der2(GammaDataLength,1) = (chi_inverse(GammaDataLength)-
chi_inverse(GammaDataLength-1))/(Data(GammaDataLength+extra,1)-
Data(GammaDataLength-1+extra,1));

%Divide the derivative by the spontaneous magnetization, then do a linear fit
c_i_derc_i = chi_inverse./der2;
p = polyfit(GammaData(1:GammaDataLength,1),c_i_derc_i(1:GammaDataLength),1);
Gamma_out_KF = 1/p(1);
Tc_Gamma_KF = abs(p(2)/p(1));

diff_tc(b+1,g+1) = Tc_beta_KF-Tc_Gamma_KF;
gamma_inter(b+1,g+1) = Gamma_out_Intercept;
diff_gamma_inter(b+1,g+1) = (Gamma_out_Intercept-Gammain);
beta_inter(b+1,g+1) = Beta_out_Intercept;
diff_beta_inter(b+1,g+1) = (Beta_out_Intercept-Betain);
gamma_kf(b+1,g+1) = Gamma_out_KF;
diff_gamma_kf(b+1,g+1) = (Gamma_out_KF-Gammain);
beta_kf(b+1,g+1) = Beta_out_KF;
diff_beta_kf(b+1,g+1) = (Beta_out_KF-Betain);

   end

end
dlmwrite('GdFe54_diff_gamma_inter', diff_gamma_inter)
dlmwrite('GdFe54_diff_beta_inter', diff_beta_inter)
dlmwrite('GdFe54_diff_gamma_kf', diff_gamma_kf)
dlmwrite('GdFe54_diff_beta_kf', diff_beta_kf)
dlmwrite('GdFe54_diff_tc', diff_tc)
```